# Photo-Uncaging of a Microtubule-Targeted Rigidin Analogue in Hypoxic Cancer Cells and in a Xenograft Mouse Model

Rixel, V.H.S. van; Ramu, V.; Auyeung, A.B.; Beztsinna, N.; Leger, D.Y.; Lameijer, L.N.; ... ; Bonnet, S.

JACS JOURNAL OF THE AMERICAN CHEMICAL SOCIETY

Article

Cite This: J. Am. Chem. Soc. 2019, 141, 18444−18454

pubs.acs.org/JACS

# Photo-Uncaging of a Microtubule-Targeted Rigidin Analogue in Hypoxic Cancer Cells and in a Xenograft Mouse Model

Vincent H. S. van Rixel,[†] Vadde Ramu,[†] Austin B. Auyeung,[†] Nataliia Beztsinna,[†] David Y. Leger,[§] Lucien N. Lameijer,[†] Stan T. Hilt,[‡] Sylvia E. Le Dévédec,[‡] Tugba Yildiz,[∥] Tania Betancourt,[∥,⊥] M. Brenton Gildner,[⊥] Todd W. Hudnall,[⊥] Vincent Sol,[§] Bertrand Liagre,[§] Alexander Kornienko,*[,⊥] and Sylvestre Bonnet*[,†]

[†]Leiden Institute of Chemistry and [‡]Leiden Academic Centre for Drug Research, Leiden University, Einsteinweg 55, 2333CC Leiden, The Netherlands

[§]Laboratoire PEIRENE EA7500, Faculté de Pharmacie, Université de Limoges, 2 rue du Dr Marcland, 87025 Limoges, France

[∥]Materials Science, Engineering, and Commercialization Program and [⊥]Department of Chemistry and Biochemistry, Texas State University, San Marcos, Texas 78666, United States

Supporting Information

**ABSTRACT:** Marine alkaloid rigidins are cytotoxic compounds known to kill cancer cells at nanomolar concentrations by targeting the microtubule network. Here, a rigidin analogue containing a thioether group was "caged" by coordination of its thioether group to a photosensitive ruthenium complex. In the dark, the coordinated ruthenium fragment prevented the rigidin analogue from inhibiting tubulin polymerization and reduced its toxicity in 2D cancer cell line monolayers, 3D lung cancer tumor spheroids (A549), and a lung cancer tumor xenograft (A549) in nude mice. Photochemical activation of the prodrug upon green light irradiation led to the photosubstitution of the thioether ligand by water, thereby releasing the free rigidin analogue capable of inhibiting the polymerization of tubulin. In cancer cells, such photorelease was accompanied by a drastic reduction of cell growth, not only when the cells were grown in normoxia (21% $O_2$) but also remarkably in hypoxic conditions (1% $O_2$). *In vivo*, low toxicity was observed at a dose of 1 mg·kg$^{-1}$ when the compound was injected intraperitoneally, and light activation of the compound in the tumor led to 30% tumor volume reduction, which represents the first demonstration of the safety and efficacy of ruthenium-based photoactivated chemotherapy compounds in a tumor xenograft.

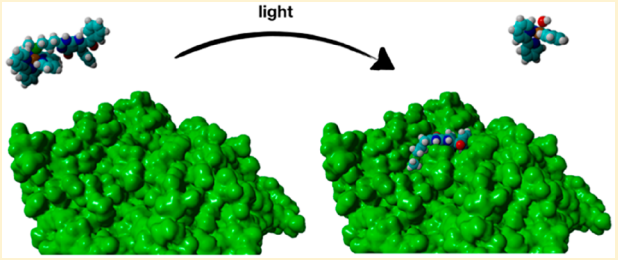


## INTRODUCTION

Microtubules play an essential role in mitosis, specifically in the separation of duplicated chromosomes before the cell divides.[1] This feature makes them a useful target for novel chemotherapeutic agents, where selective killing of highly dividing cells is essential. One of the most successful microtubule-targeting agents used in the clinic is paclitaxel, which is employed to treat various forms of breast, ovarian, and non-small cell lung cancer. Paclitaxel interferes with microtubule dynamics leading to apoptosis and cell death.[2] However, paclitaxel-based therapy is plagued with side-effects which include neutropenia, neurotoxicity, and disturbances in cardiac rhythm, among others.[3,4] Additionally, cancer cell resistance to paclitaxel therapy limits its clinical efficacy, making the development of alternative microtubule-targeting agents or strategies an important area of cancer research. Some of us have been investigating analogues derived from marine alkaloid rigidins, isolated from the tunicate *Eudistoma cf. rigida*, as novel microtubule-targeting agents.[5,6] Extensive structure−activity relationship studies revealed analogues that kill cancer cells at low-nanomolar concentrations and induce significant tumor growth reduction *in vivo*. However, as with any microtubule-targeting agents, it could be anticipated that the uptake by the healthy tissues would result in side-effects limiting the progression of a potential drug candidate through preclinical or clinical development.

To address these obstacles early on, we investigated the potential of a rigidin analogue containing a thioether group (**1**, Figure 1) to serve as a ligand for light-cleavable ruthenium complex $[\mathbf{2}]^{2+}$ (Figure 1). This strategy is often referred to as photoactivated chemotherapy (PACT).[7−16] In PACT, the inactive prodrug is activated locally by light irradiation via a bond photocleavage reaction.[13] In the dark, the positively charged metal complex poorly interacts with its target, while upon light irradiation, a photosubstitution reaction leads to the release of the free and active cytotoxic drug. PACT derives from a clinically approved phototherapy technique called photodynamic therapy (PDT).[13,17,18] In both cases, toxicity is generated by the light irradiation of a photoactive compound.

**Received:** July 8, 2019
**Published:** October 18, 2019






DOI: 10.1021/jacs.9b07225
J. Am. Chem. Soc. 2019, 141, 18444−18454

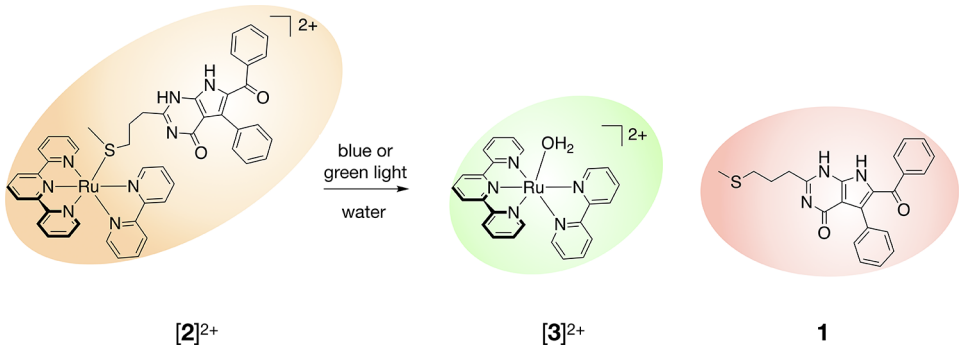


**Figure 1.** Photochemical release of rigidin-thioether **1**[5] from ruthenium-based PACT compound $[\mathbf{2}]^{2+}$.

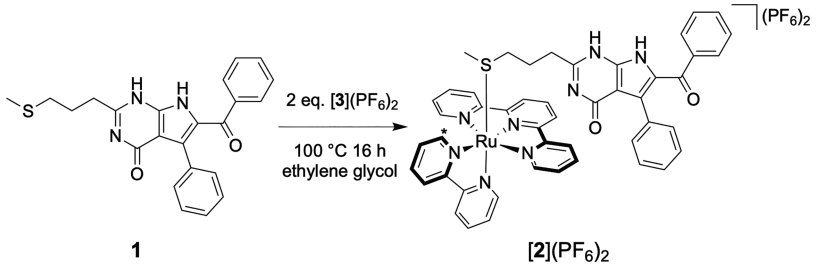


**Figure 2.** Synthesis of $[\mathbf{2}](PF_6)_2$. * indicates the A6 proton of the 2,2′-bipyridine (bpy) ligand.

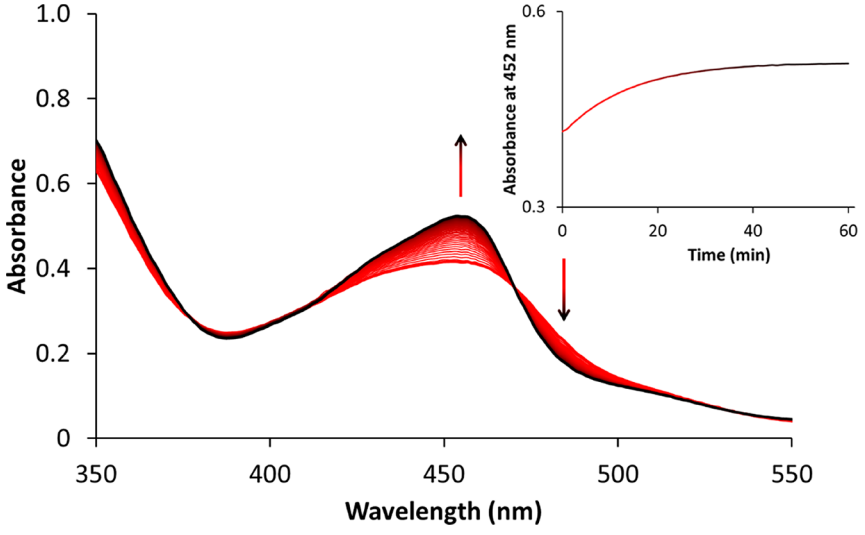


**Figure 3.** Evolution of the electronic absorption spectra of a solution of $[\mathbf{2}](PF_6)_2$ in acetonitrile upon green light irradiation under nitrogen ($\lambda$ = 530 nm, $\Delta\lambda_{1/2}$ = 17 nm, 6.0 mW, photon flux $4.1\times 10^{-8}$ mol·s$^{-1}$). Time: 0 min (red curve) to 30 min (black curve). Conditions: $[Ru]_0$ = 50 $\mu$M, irradiated volume 3.0 mL, temperature 293 K.

Since light is delivered directly to the tumor, PDT was shown to generate less systemic toxicity for cancer patients, compared to traditional chemotherapy.[19,20] However, there is an essential difference between PDT and PACT. In PDT, a light-irradiated photosensitizer generates cytotoxicity via energy or electron transfer of the excited prodrug molecule to the $O_2$ present in the irradiated tumor tissues. PDT is hence highly efficient in well-oxygenated tumors, but it often fails in hypoxic tumors, where low $O_2$ concentrations limit the photogeneration of oxidative stress.[21] On the contrary, in PACT the light activation mechanism is based on $O_2$-independent bond cleavage photoreaction, so PACT should, in principle, allow for the development of anticancer phototherapies that are independent of the intratumoral $O_2$ concentration and thus suitable for the treatment of hypoxic tumors.[22,23] Considering that oxygen-deficient tumors are very difficult to treat by either PDT, radiation therapy,[24] chemotherapy,[25,26] or immunotherapy,[27] developing new treatment modalities that are nontoxic in the dark, that upon light irradiation focus on a well-established cancer target, and that remain efficacious under hypoxic conditions, represents an important goal in oncology. The present work investigates the use of $[\mathbf{2}](PF_6)_2$ as a new PACT complex releasing microtubule-targeting rigidin compound **1** under green light irradiation (Figure 1). We provide quantitative phototoxicity studies *in vitro* under normoxia (21% $O_2$) and hypoxia (1% $O_2$) demonstrating efficient light activation in low $O_2$ concentrations. In addition, we established the first demonstration of the light-activation of a ruthenium-


DOI: 10.1021/jacs.9b07225
J. Am. Chem. Soc. 2019, 141, 18444−18454

based PACT compound in 3D tumor spheroids and in human lung cancer (A549) xenografts in nude mice.

## RESULTS

**Synthesis of the Caged Microtubule Inhibitor.** Complex $[Ru(tpy)(bpy)(\mathbf{1})](PF_6)_2$ ($[\mathbf{2}](PF_6)_2$) was synthesized by reacting thioether-containing microtubule inhibitor **1** with 2 equiv of $[Ru(tpy)(bpy)(OH_2)](PF_6)_2$ ($[\mathbf{3}](PF_6)_2$, Figures 1 and 2). $^1$H NMR spectroscopy in $CD_3OD$ showed the characteristic upfield shift at 1.47 ppm of the coordinated SMe group (methylthioether moieties typically appear at >2.0 ppm in protic solvents).[28] Additional NMR spectroscopy, high-resolution mass spectrometry, and elemental analysis, unequivocally demonstrated the analytical purity of $[\mathbf{2}](PF_6)_2$. Unlike **1**, which is essentially hydrophobic (log $P$ > 4.0), $[\mathbf{2}](PF_6)_2$ was dramatically more water-soluble (log $P$ = −0.21; see the Supporting Information). This result highlights one of the recognized advantages of ruthenium-based photocaging groups: Their ability to solubilize in water hydrophobic organic inhibitors.[23]

**Photochemistry.** Green ($\lambda_{irr}$ = 530 nm) light irradiation of a solution of $[\mathbf{2}](PF_6)_2$ in acetonitrile under an inert atmosphere of dinitrogen resulted in a significant increase of the absorbance at 452 nm and a slight shift of the maximum of the singlet metal-to-ligand charged transfer ($^1$MLCT) band from 452 to 454 nm (Figure 3). Under these conditions, a steady state was obtained after 30 min (inset in Figure 3). Mass spectrometry (MS) of the solution after light irradiation showed peaks at $m/z$ = 266.4 corresponding to $[Ru(tpy)(bpy)(CH_3CN)]^{2+}$ (calcd $m/z$ = 266.1, Figure S1), whereas MS of the dark control showed a major signal at $m/z$ = 447.0 corresponding to $[\mathbf{2}]^{2+}$ (calcd $m/z$ = 447.1, Figure S1). Thus, under green light irradiation, ligand **1** was photosubstituted by a solvent molecule, with a quantum yield $\Phi_{530}$ of 0.0038. Similar evolutions were observed using blue light irradiation (450 nm, Figure S2) and in such conditions a modestly higher photosubstitution quantum yield $\Phi_{450}$ of 0.0055 was obtained. When monitored by $^1$H NMR in $CD_3CN$ under white light irradiation, the photoreaction led after 5 min to a shift of the characteristic A6 proton (Figure S3) at 9.66 ppm on the bipyridine ligand to 9.59 ppm, characteristic for $[Ru(tpy)(bpy)(CH_3CN)]^{2+}$. Meanwhile, the initial singlet peak at 1.32 ppm characteristic for the coordinated SMe was fully replaced by a singlet peak at 2.54 ppm for noncoordinated **1**. Additionally, the spin−lattice relaxation times ($T_1$) measured on pre- and postphotoreaction of $[\mathbf{2}]^{2+}$ were consistent with the photorelease of free inhibitor **1**. For example, the $T_1$ times measured for the SMe and the adjacent methylene unit before the photoreaction were markedly shorter at 1.025 and 0.680 s, respectively, when compared to the postphotoreaction measurements (1.820 and 1.724 s, respectively, Figure S4). This difference is consistent with the $Ru^{2+}$ center aiding in relaxation of the thiomethyl and methylene protons when the inhibitor is coordinated.[29−31] Similarly, we observed an increase in the $T_1$ of the A6 proton from 2.150 to 3.205 s after photolysis, consistent with molecular weight; therefore, the size of the $Ru^{2+}$ complex decreases when inhibitor **1** is replaced by the solvent $CH_3CN$.[32] Collectively, all data showed the full and selective conversion of $[\mathbf{2}]^{2+}$ into free inhibitor **1** plus $[Ru(tpy)(bpy)(CH_3CN)]^{2+}$, i.e., a solvent-coordinated ruthenium adduct (Figure S3).[33] When the same light irradiation reaction was performed in demineralized water and followed by UV−vis spectroscopy, Rayleigh scattering occurred quickly due to precipitation of free ligand **1**, which is poorly soluble in water (maximum solubility is 10 μM in demineralized water, see Figure S5). Overall, it can be concluded that the Ru−S bond of $[\mathbf{2}]^{2+}$ is photoactivatable in $CH_3CN$ and aqueous solution using either blue, green, or white light.

**Tubulin Polymerization Assay.** In order to investigate how caging and photoactivation influences the ability of compound $[\mathbf{2}](PF_6)_2$ to interact with its biological microtubule target, a fluorescence-based tubulin polymerization assay was utilized to compare the tubulin polymerization properties of $[\mathbf{2}](PF_6)_2$ in the dark and under light irradiation. In this assay, tubulin polymerization leads to a marked increase of the fluorescence intensity. As expected, paclitaxel induced rapid polymerization of tubulin, whereas colchicine suppressed it (Figure 4).[5] It was further found that tubulin polymerization

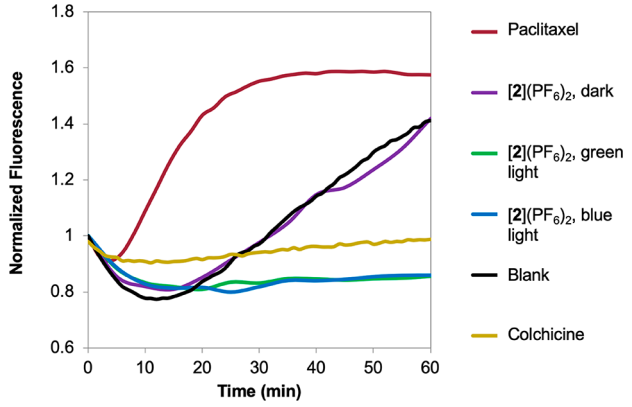


**Figure 4.** Results of tubulin polymerization assay. Raw fluorescence was normalized by initial fluorescence for each sample. Samples consist of the caged inhibitor $[\mathbf{2}](PF_6)_2$ (25 μM) left in the dark or irradiated with green or blue light. Paclitaxel (3 μM) and colchicine (6 μM) were utilized as tubulin polymerization enhancer and suppressor controls, respectively. Irradiation time: 30 min.

was completely inhibited with the caged drug $[\mathbf{2}](PF_6)_2$ that had been irradiated with either blue or green light (38 J·cm$^{-2}$). This observation suggests that exposure to light liberates the active agent, thereby enabling its inhibitory effect. The caged control (not exposed to light) showed a behavior that is typically associated with a substance that neither inhibits nor promotes tubulin polymerization as expected, suggesting that the caged drug $[\mathbf{2}](PF_6)_2$ is not active. In other words, photochemical uncaging of the inhibitor in $[\mathbf{2}](PF_6)_2$ efficiently recovers the inhibiting properties of ligand **1**.

**Light Activation of $[\mathbf{2}](PF_6)_2$ Inhibits Tubulin Polymerization in Normoxic A549 Cells.** Since the chemical tubulin polymerization assay demonstrated that caged drug $[\mathbf{2}](PF_6)_2$ completely inhibited the polymerization of tubulin after light irradiation, an immunofluorescent staining assay was performed in A549 cells to validate whether such light-controlled tubulin polymerization inhibitory effect would also occur in living cells and at which concentration such inhibition would occur. A549 cells were grown under normoxia, treated with a range of concentrations of $[\mathbf{2}](PF_6)_2$ (1, 5, 10, 20, 50, and 100 μM) and either irradiated with green light or left in the dark. After 4 or 16 h of light irradiation, both dark and irradiated plates were imaged after immunostaining the nuclei (blue), α-tubulin (green), and F-actin (red). As shown in Figure 5, irradiation of $[\mathbf{2}](PF_6)_2$ caused a dose-dependent


DOI: 10.1021/jacs.9b07225
J. Am. Chem. Soc. 2019, 141, 18444−18454

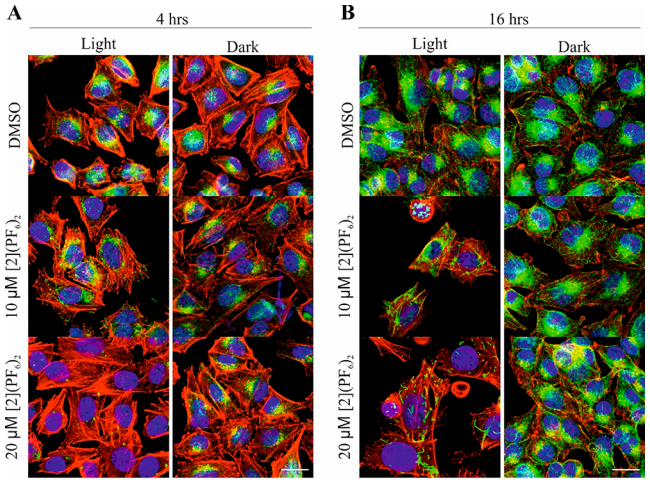


**Figure 5.** Immunofluorescent staining of A549 cancer cells treated with $[\mathbf{2}](PF_6)_2$ or vehicle control, irradiated with green light (530 nm) or left in the dark, and imaged at 4 h (A) or 16 h (B) after light activation. Light activation of the caged drug $[\mathbf{2}](PF_6)_2$ induces microtubules breakdown in a dose-dependent fashion, while under the dark regime, the microtubule cytoskeleton is unaffected. Staining: $\alpha$-tubulin (green), DNA (blue), and F-actin (red). Scale bars: 20 $\mu$m. See Figures S7–S9 for the whole concentration range and for individual channels.

depolymerization of the microtubules, while the dark regime showed no effect on microtubule polymerization even at high concentrations (see Figures S7–S9). Interestingly, the actin cytoskeleton did not show any major modification by light activation or in the dark, which shows the specificity of tubulin polymerization inhibition by photoreleased ligand **1**. Photoactivation of 20 $\mu$M of $[\mathbf{2}](PF_6)_2$ was sufficient to completely and specifically break down the microtubule cytoskeleton 4 h after irradiation (Figure 5A). Even after 16 h, the polymerization was still strongly impaired in the light-activated cells (Figure 5B). Those data indicate that in living A549 cancer cells the caged compound $[\mathbf{2}](PF_6)_2$ is after light activation highly specific and efficient inhibitor of tubulin polymerization, which is consistent with the release of ligand **1** inside the cells.

**(Photo)toxicity Studies under Normoxia.** An *in vitro* photocytotoxicity assay was performed to demonstrate whether the activity of $[\mathbf{2}](PF_6)_2$ could be controlled with light activation in living cells (*in cellulo*) and how it would translate in terms of cytotoxicity. The cytotoxicities of **1**, $[\mathbf{2}](PF_6)_2$, caging group $[\mathbf{3}](PF_6)_2$, and cisplatin were investigated first under normal dioxygen concentration (21% $O_2$) against skin (A375 and A431) and lung (A549) cancer cell lines, as well as against MRC-5 noncancer cell line (Table 1). $[\mathbf{3}](PF_6)_2$ was included in the assay to ensure that cytotoxicity of $[\mathbf{2}](PF_6)_2$ after light activation does not originate from the metal cage; cisplatin was tested as positive control. Cell growth inhibition effective concentrations ($EC_{50}$), defined as the compound concentration that reduces cell viability by 50% compared to untreated cells, were measured in the dark and after light activation following a protocol adapted from Hopkins et al.[34] All results are shown in Table 1. In the dark, $EC_{50}$ values between 0.16 and 0.23 $\mu$M were found for **1** in A375, A431, and MRC-5 cells, and a higher value of 6.5 $\mu$M was found for A549 cells. Compound $[\mathbf{3}](PF_6)_2$ showed no activity across all tested cell lines, which is in agreement with previous findings,[35] while treatment with cisplatin resulted in $EC_{50}$ values in the expected micromolar range, i.e., between 0.87 and 3.1 $\mu$M. For caged compound $[\mathbf{2}](PF_6)_2$ in the dark, $EC_{50}$ values of 7–14 $\mu$M in A375, A431, and MRC-5 cells were observed, while for A549 cells an $EC_{50}$ value of 35 $\mu$M was measured. Thus, caging of **1** with the $[Ru(tpy)(bpy)]^{2+}$ moiety strongly inhibited, up to 83 times for MRC-5 cells, the cytotoxicity of ligand **1** in the dark.

Green light (520 nm) was chosen for photochemical activation since it is much less toxic *in vitro* and *in vivo* to living cells than blue light, despite the slightly lower activation quantum yield of $[\mathbf{2}](PF_6)_2$ with green light versus blue light.[34,36,37] Preliminary studies in a 96-well plate (Figure S6) demonstrated that in the conditions of our cell-irradiation setup (21 mW·cm$^{-2}$), a 30 min irradiation time, corresponding to a dose of 38 J·cm$^{-2}$, was necessary to completely activate the highest concentration of $[\mathbf{2}](PF_6)_2$ used in the assay (60 $\mu$M). While a 38 J·cm$^{-2}$ dose of green light did not induce photocytotoxicity or change the cytotoxicity of uncaged inhibitor **1**, caging complex $[\mathbf{3}](PF_6)$, or cisplatin, the effect observed when caged inhibitor $[\mathbf{2}](PF_6)_2$ was irradiated under 21% $O_2$ was remarkable for all cell lines tested. $EC_{50}$ values for A375, A431, A549, and MRC-5 cells were 0.33, 0.49, 9.2, and 0.67 $\mu$M, leading to phototoxic indices of 21, 29, 4, and 12, respectively. Figure 6 shows, as an example, the dose–response curves for A431 cells treated with **1** (brown curve), $[\mathbf{2}](PF_6)_2$ in the dark (black curve), $[\mathbf{2}](PF_6)_2$ irradiated with green light (green curve), and $[\mathbf{3}](PF_6)_2$ in the dark (gray curve). For most cell lines, the toxicity of $[\mathbf{2}](PF_6)_2$ after light activation was slightly lower than that of **1**, which may be due to the lower drug uptake in the dark for the caged, positively charged compound, while **1** is very lipophilic and may easily penetrate the cell. Overall, the data suggests that $[Ru(tpy)(bpy)]^{2+}$ is an excellent photocaging agent for **1** as coordination to ruthenium strongly reduces the cytotoxicity of **1** in the dark, while photocleavage, when performed in living cells, restores the high toxicity typical for ligand **1**.

**Effect of Hypoxia.** Although significant photoindices of $[\mathbf{2}](PF_6)_2$ were measured in normoxic cancer cells, the true added value of PACT compounds is for treating hypoxic tumors, where other cancer treatment modalities such as PDT or radiation therapy often fail.[24,26,27,38,39] Thus, the cytotoxicity of $[\mathbf{2}](PF_6)_2$, $[\mathbf{3}](PF_6)_2$, **1**, and cisplatin were tested under hypoxia (1% $O_2$) in the same cancer cell lines. The cells were cultivated for 2 weeks under a 1% $O_2$ concentration before starting the cytotoxicity assay, which was fully performed under hypoxia, including light irradiation, using a setup reported recently.[23] The results are reported in Table 1. All three compounds, **1**, $[\mathbf{2}](PF_6)_2$, and cisplatin, were less active under hypoxia than under normoxia, which is indicative of the known resistance of hypoxic cancer cells against chemotherapeutic drugs.[26,39] Most importantly, however, in A549 the $EC_{50}$ of $[\mathbf{2}](PF_6)_2$ in the dark and under green light irradiation increased by the same ratio when going from normoxia to hypoxia, resulting in almost identical photoindices under hypoxia compared to normoxia (4.1 vs 4.0). In A375 and A431, the photoindices of $[\mathbf{2}](PF_6)_2$ remained high under hypoxia, also showing that the photoactivation of this compound was independent from the oxygen concentration in the cell. This result is one of the rare demonstrations that PACT agents are equally activated under hypoxia and normoxia,[22,23] and hence show promise for the phototherapeutic treatment of hypoxic tumors.

Curiously, MRC-5 cells were very sensitive to both drugs **1** and light-activated $[\mathbf{2}](PF_6)_2$, even more than the A549 cells.


DOI: 10.1021/jacs.9b07225
J. Am. Chem. Soc. 2019, 141, 18444–18454

**Table 1. Cytotoxicity in the Dark and under Green Light Irradiation in Normoxic (21% $O_2$) and Hypoxic (1% $O_2$) Conditions**[a]

| | | [2](PF6)2 | | | | | [3](PF6)2 | | | | 1 | | | | | cisplatin | | | | |
|---|---|---|---|---|---|---|---|---|---|---|---|---|---|---|---|---|---|---|---|---|
| cell line | % $O_2$ | $EC_{50}$ dark (μM) | $CI_{95}$ (μM) | $EC_{50}$ GL (μM)[b] | $CI_{95}$ (μM) | PI[b] | $EC_{50}$ dark (μM) | $CI_{95}$ (μM) | $EC_{50}$ GL (μM)[b] | $CI_{95}$ (μM) | $EC_{50}$ dark (μM) | $CI_{95}$ (μM) | $EC_{50}$ GL (μM)[b] | $CI_{95}$ (μM) | PI[b] | $EC_{50}$ dark (μM) | $CI_{95}$ (μM) | $EC_{50}$ GL (μM)[b] | $CI_{95}$ (μM) | PI[b] |
| **A549** | 21% | 35 | +8.7 −11 | 9.2 | +4.0 −7.1 | 4.0 | >100 | n.a. | >100 | n.a. | 6.5 | +1.6 −0.5 | 3.4 | +0.5 −0.5 | 1.9 | 1.3[b] | +0.4 −0.6 | 2.0 | +0.3 −0.2 | <1 |
| | 1% | 55 | +13 −10 | 14 | +3.7 −2.9 | 4.1 | >100 | n.a. | >100 | n.a. | 6.4 | +2.5 −1.8 | 6.6 | +2.8 −1.9 | ~1 | 4.7 | +0.8 −0.7 | 4.4 | +0.9 −0.8 | ~1 |
| **MRC-5** | 21% | 8.1 | +1.4 −1.7 | 0.67 | +0.3 −0.5 | 12 | >100 | n.a. | >100 | n.a. | 0.17 | +0.07 −0.13 | 0.34 | +0.2 −0.3 | <1 | 1.5[b] | +0.2 −0.2 | 2.2 | +0.2 −0.3 | <1 |
| | 1% | 21 | +7.9 −5.8 | 4.4 | +1.8 −1.3 | 4.8 | >100 | n.a. | >100 | n.a. | 0.9 | +0.7 −0.4 | 0.8 | +0.8 −0.4 | ~1 | 9.4 | +5.7 −3.6 | 6.7 | +2.0 −1.6 | 1.4 |
| **A375** | 21% | 6.8 | +1.7 −1.4 | 0.33 | +0.2 −0.1 | 21 | >100 | n.a. | >100 | n.a. | 0.16 | +0.07 −0.05 | 0.20 | +0.1 −0.06 | 1.2 | 0.85 | +0.08 −0.07 | 0.87 | +0.06 −0.06 | 1.0 |
| | 1% | >50 | n.a. | 3.1 | +0.9 −0.7 | >16 | >75 | n.a. | >75 | n.a. | 1.4 | +0.9 −0.5 | 0.70 | +0.2 −0.2 | 1.9 | 2.8 | +0.9 −0.7 | 2.8 | +0.4 −0.3 | 1.0 |
| **A431** | 21% | 14 | +3.9 −3.0 | 0.49 | +0.06 −0.05 | 29 | >100 | n.a. | >100 | n.a. | 0.23 | +0.03 −0.02 | 0.24 | +0.04 −0.03 | 1.0 | 2.8 | +0.3 −0.3 | 3.1 | +0.4 −0.4 | 1.1 |
| | 1% | >50 | n.a. | 4.2 | +3.3 −1.9 | >12 | >75 | n.a. | >75 | n.a. | 1.1 | +1.1 −0.55 | 0.83 | +0.2 −0.1 | 1.3 | 2.5 | +0.3 −0.3 | 2.9 | +0.3 −0.3 | 1.1 |

[a]Cell growth inhibition effective concentrations ($EC_{50}$ Values in μM) with 95% confidence interval ($CI_{95}$ in μM) for **1**, [**2**]$(PF_6)_2$, [**3**]$(PF_6)_2$, and cisplatin, on lung (A549) and skin (A431, A375) cancer cell lines, and on MRC-5 "non-cancer" cell line. The photo index (PI), defined as $EC_{50,dark}/EC_{50,light}$, is also indicated. [b]GL = green light (522 nm), 21 mW·cm$^{-2}$ for 30 min under normoxia or 16 mW·cm$^{-2}$ under hypoxia (dose 38 J·cm$^{-2}$). Treatment-to-irradiation time was 24 h in both normoxic and hypoxic conditions.



J. Am. Chem. Soc. 2019, 141, 18444−18454
DOI: 10.1021/jacs.9b07225

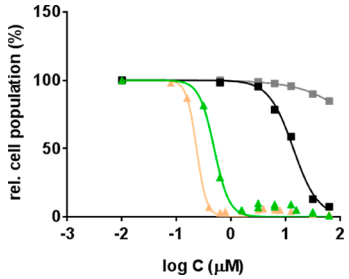


**Figure 6.** Dose−response curves for A431 cells incubated with **1** in the dark (light brown), [**2**](PF$_6$)$_2$ in the dark (black), [**2**](PF$_6$)$_2$ with green light irradiation (green), and [**3**](PF$_6$)$_2$ in the dark (grey). Phototoxicity assay: cells seeded at $8 \times 10^3$ cells/well at $t$ = 0 h, treated at $t$ = 24 h, irradiated at $t$ = 30 h, and SRB assay performed at $t$ = 96 h. Conditions: $T$ = 37 °C, v/v % $CO_2$ = 7%, $\lambda_{irr}$ = 520 nm, light dose = 38 J·cm$^{-2}$.

This sensitivity was particularly high under normoxia, where it resulted in a thrice higher photoindex (12) compared to hypoxia, where the photoindex (4.8) was similar to that found in A549 cells. To investigate whether these differences may be due to different cell growth rates between MRC-5 and A549, the growth rate of both cell lines was determined under normoxia and hypoxia, over a 4 week period (Figures 7 and S11). After 1 week of culture under normoxia, the cells were split in to two parts and further cultured either under normoxia (21% $O_2$) or hypoxia (1% $O_2$). At the beginning of weeks 2, 3, and 5, one portion of each cell stock was seeded in 96-well plates, cultured for 1 week, and fixed at 24, 72, 120, and 196 h after seeding. At the end of each week, the cell population at fixation time, relative to the 24 h time point of the same week, was assayed using the sulforhodamine B (SRB) assay.[40] A549 cells showed a faster growth rate in normoxia compared to that in hypoxia during weeks 2 and 3. On the contrary, MRC-5 cells showed faster growth in hypoxic compared to normoxic conditions during weeks 2 and 3, and evened out by week 5. Hypoxia is a traumatic event, which triggers a variety of physiological actions, such as energy metabolism, autophagy, cell motility, angiogenesis, and erythropoiesis. An important cellular effect of hypoxia is as a modulator of cell proliferation.[41] For many cell types, including A549, hypoxia was reported to induce decreased cell proliferation,[42,43] since an increase in the number of cells would result in increased oxygen demand and accompanying hypoxic stress.[41] MRC-5 fibroblasts are mostly responsible for extracellular matrix production in lungs.[44] The increased growth rate in hypoxia of lung fibroblasts, including MRC-5 cells, has been documented, but its mechanism is not well understood.[45] It has been hypothesized that increased proliferation of pulmonary fibroblasts is mediated through the hypoxia-induced nuclear factor activated T-cell (NFAT) pathway and is dependent on HIF-2$\alpha$ rather than HIF-1$\alpha$.[46] The MRC-5 growth pattern in hypoxia could be due to a hypoxia-induced

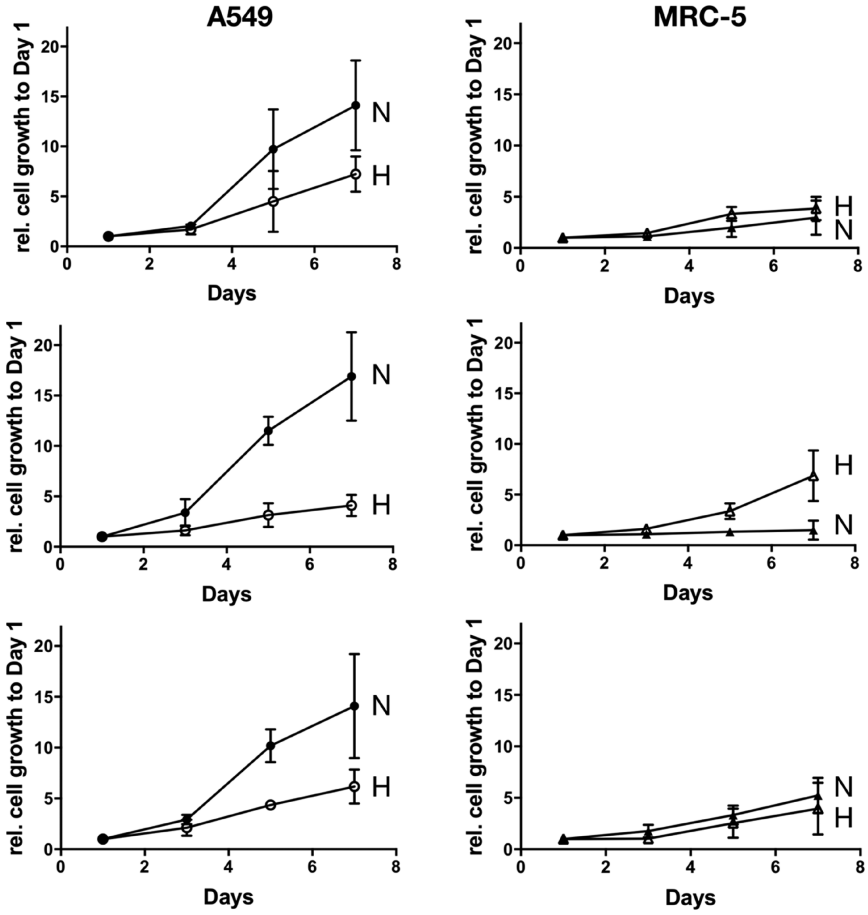


**Figure 7.** Growth curves for week 2 (top), week 3 (middle), and week 5 (bottom) for A549 (left, circles) and MRC-5 (right, triangles) cell lines under normoxia (21% $O_2$, N, filled symbols) and hypoxia (1% $O_2$, H, empty symbols). Time line of the experiment shown in Figure S11. Seeding density for all cell lines was $5 \times 10^3$ cells/well. Data averaged over **2** or **3** independent experiments.



DOI: 10.1021/jacs.9b07225
J. Am. Chem. Soc. 2019, 141, 18444−18454

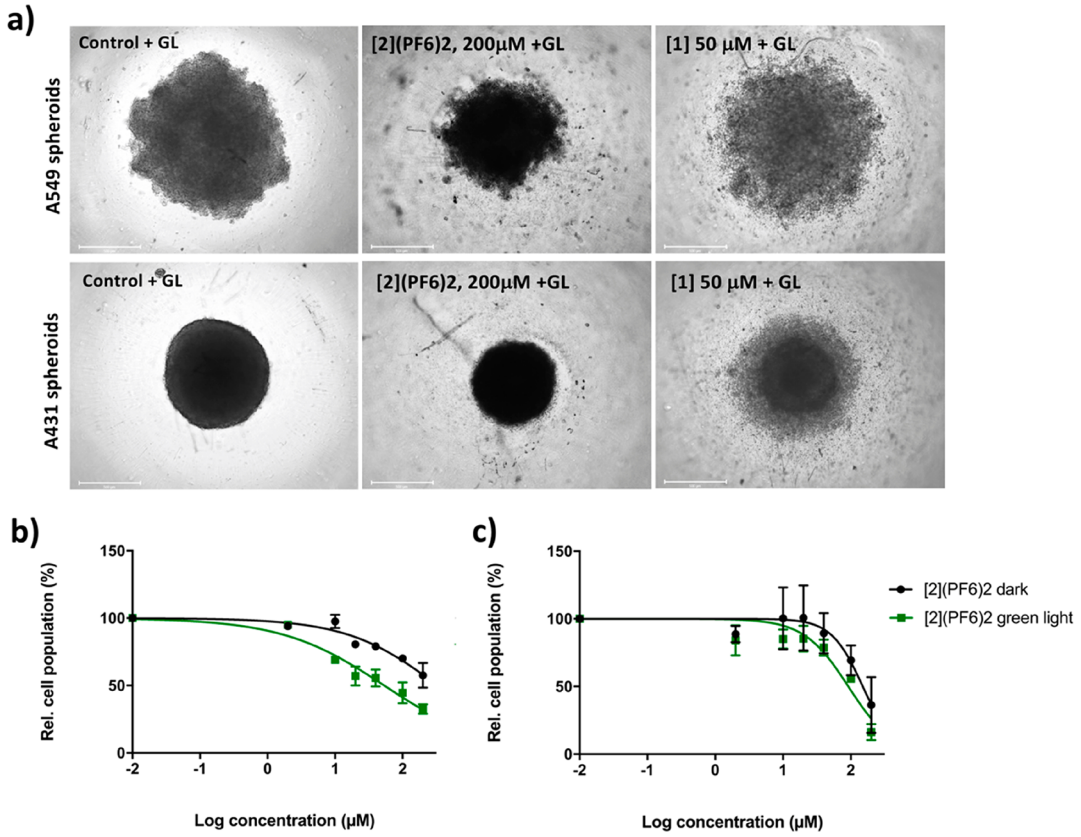


**Figure 8.** (a) Bright-field microscopy photographs of A549 and A431 spheroids grown in normoxic conditions, treated with vehicle control, 200 $\mu$M of $[\mathbf{2}](PF_6)_2$, or 50 $\mu$M of **1**, and irradiated with green light (GL, 530 nm, 90 min, light dose 37 J·cm$^{-2}$). Dose–response curve for A431 (b) and A549 (c) spheroids incubated with $[\mathbf{2}](PF_6)_2$ and kept in the dark (black) or activated by green light (GL). Phototoxicity assay: cells seeded at $2 \times 10^2$ cells/well at $t$ = 0 days, treated at $t$ = 4 days, and irradiated at $t$ = 5 days. Cell Titer Glo 3D viability assay performed at $t$ = 7 days. Conditions: $T$ = 37 °C, v/v % $CO_2$ = 7%. Scale bar 500 $\mu$M.

transformation into cancer associated fibroblasts (CAF).[47] Clearly, the phototoxicity of $[\mathbf{2}](PF_6)_2$ in A549 cancer cells is not directly dependent on cell growth rate, as the lower growth rate under hypoxia led to identical photoindices (PI), while in MRC-5 "non-cancer" cells a higher growth rate was accompanied by a lower PI.

**(Photo)toxicity in 3D Tumor Spheroids.** In view of the excellent phototoxicity of $[\mathbf{2}](PF_6)_2$ in 2D monolayers of hypoxic and normoxic cells, 3D tumor spheroids were chosen as an additional *in vitro* model to test the (photo)toxicity of $[\mathbf{2}](PF_6)_2$. 3D models have become important for *in vitro* testing as they are a better model for clinical tumors in terms of light, nutrient, and drug penetration and as they can give valuable insight for *in vivo* experiments. 3D spheroids were hence formed from A549 and A431 cancer cells in suspension using ultralow attachment 96-well plates. The spheroids were first seeded at 200 cells/well, treated at day 4 with **1** or $[\mathbf{2}](PF_6)_2$, irradiated with green light after 24 h of incubation (or kept in the dark for the dark plate), and further incubated in the dark until day 7. The spheroids were imaged (Figure 8a) and their viability was assessed using the Cell Titer Glo 3D ATP quantification (Figure 8b,c and Table 2). Compared to 2D experiments, the $EC_{50}$ values were higher for all tested conditions. Without green light irradiation, the $EC_{50}$ of $[\mathbf{2}](PF_6)_2$ was 330 $\mu$M in A431 and 150 $\mu$M in A549, which are almost 24 and 4 times higher, respectively, than the values found in 2D for the same cell lines. The particularly high $EC_{50}$ found in A431 spheroids correlates well with the compact morphology of spheroids of this cell line, which may prevent charged compound $[\mathbf{2}](PF_6)_2$ from penetrating to the core of the spheroid. In contrast, the less compact A549 spheroids seem to let $[\mathbf{2}](PF_6)_2$ better penetrate inside the spheroid, as shown by the lower increase of the $EC_{50}$ in 3D, compared to 2D. After green light irradiation (37.2 J·cm$^{-2}$), the $EC_{50}$ of $[\mathbf{2}](PF_6)_2$ was 54 and 92 $\mu$M in A431 and A549 spheroids, i.e., 100 and 10 times higher than in 2D but 6.1 and 1.6 times

**Table 2. Cell Growth Inhibition Effective Concentrations**[a]

| cell line | seeding density (cells/well) | light dose (J·cm$^{-2}$) | $[\mathbf{2}](PF_6)_2$ $EC_{50}$ ($\mu$M) | $CI_{95}$ | PI |
|---|---|---|---|---|---|
| **A431** | 200 | 0 | 330 | −114<br>+350 | 6.1 |
| | | 37 | 54 | −14<br>+23 | |
| **A549** | 200 | 0 | 150 | −38<br>+76 | 1.6 |
| | | 37 | 92 | −21<br>+27 | |
| **A549** | 500 | 0 | 205 | −222<br>+57 | 3.2 |
| | | 83 | 63.7 | −21<br>+14 | |

[a]$EC_{50}$ values in $\mu$M, with 95% confidence interval ($CI_{95}$ in $\mu$M), for $[\mathbf{2}](PF_6)_2$ and cisplatin in 3D tumor spheroids of lung (A549) and skin (A431) cancer cells. The photoindex (PI), defined as $EC_{50,dark}/EC_{50,light}$, is also indicated.



DOI: 10.1021/jacs.9b07225
J. Am. Chem. Soc. 2019, 141, 18444−18454

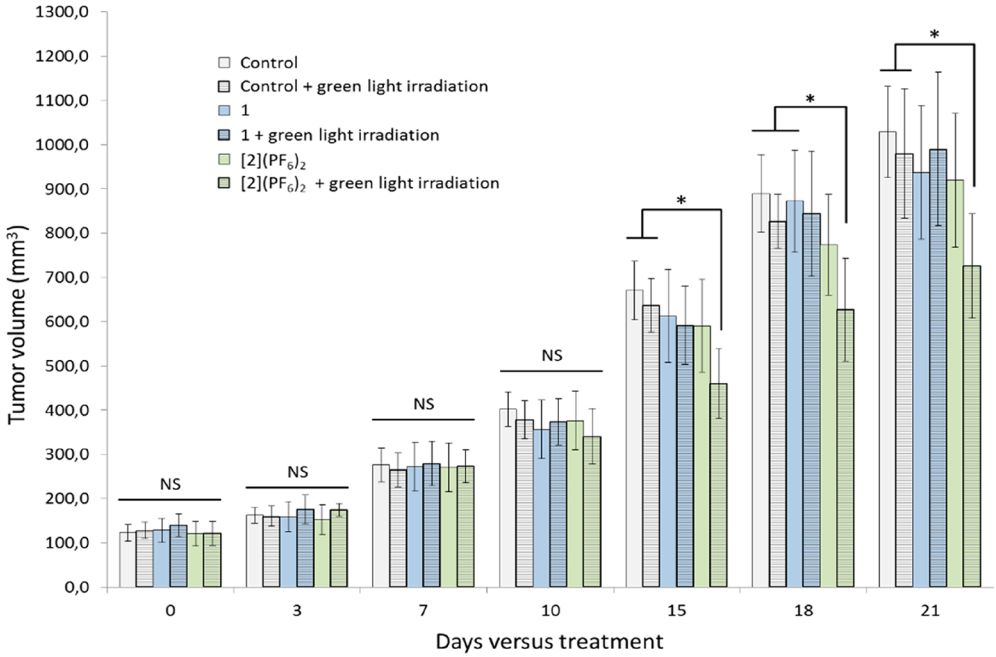


**Figure 9.** Evolution of tumor volumes of A549 cells xenografts in nude mice left untreated in the dark (gray histogram) or only irradiated with green light (gray and striated histogram); treated with **1** (1 mg·kg$^{-1}$) and either left in the dark (blue histogram) or irradiated with green light (blue and striated histogram); and treated with $[\mathbf{2}](PF_6)_2$ (1 mg·kg$^{-1}$) and either left in the dark (green histogram) or irradiated with green light (green and striated histogram). There were 5 mice per group; values are expressed as mean ± SEM ($p$ value relative to control group; *, $p < 0.05$).

lower, respectively, than in 3D and in the dark. As one could observe from the microscopy photographs in Figure 8a, the morphology of the treated spheroids was different in presence of both compounds; A549 spheroids treated with $[\mathbf{2}](PF_6)_2$ and irradiated with light were darker and had scattered dead cells around them, compared to those treated with **1**, for which an $EC_{50}$ of 140 $\mu$M was found that did not depend on the presence of light. In A431 spheroids, the spheroids treated with $[\mathbf{2}](PF_6)_2$ remained compact but showed scattered cells, while those treated with **1** ($EC_{50}$ = 15 $\mu$M) had a low-density corona surrounding a more compact core, confirming the higher 2D toxicity of **1** in this cell line ($EC_{50}$ = 0.24 $\mu$M), and its probable penetration properties due to its neutral charge. Overall, in A431 spheroids $[\mathbf{2}](PF_6)_2$ was activated by light (PI = 6.1), but the compound was rather strongly inhibited compared to 2D cell monolayers, probably due to its hydrophilicity that may preclude optimal diffusion to the core of the spheroid. For A549 spheroid, the decrease in cytotoxicity compared to 2D was significantly lower, but the photoindex was suboptimal.

As light penetration may be a stronger issue in 3D than in 2D, a second tumor spheroid experiment was repeated with A549 cells using higher light doses (83 J·cm$^{-2}$), and a clinically used drug (cisplatin) as control. In this second experiment the spheroid diameter was followed as well by bright field imaging, which also revealed a clear effect of green light irradiation for spheroids treated with $[\mathbf{2}](PF_6)_2$ (Figure S12b,c). The spheroids diameter before treatment was on average 302 ± 29 $\mu$m, while 72 h later the average spheroid diameter in nontreated group (negative control) was 477 ± 3 $\mu$m indicating spheroid growth. In contrast, treatment with $[\mathbf{2}](PF_6)_2$ or cisplatin induced a concentration-dependent decrease in spheroid size compared to that of vehicle control. In the dark, the $EC_{50}$ at day 7 for $[\mathbf{2}](PF_6)_2$ (Table 2) was 205 $\mu$M, which is only 6 times higher than that for the same cell line in 2D. The $EC_{50}$ of $[\mathbf{2}](PF_6)_2$ after green light irradiation was 64 $\mu$M, i.e., 7 times higher than that in 2D but 3.2 times lower than that in 3D and in the dark, confirming a higher photoindex of $[\mathbf{2}](PF_6)_2$ in 3D at higher light doses. Under these conditions, the $EC_{50}$ values for cisplatin were 15 times higher (30 $\mu$M), compared to the value found in 2D, irrespective of whether the cells were irradiated or not. Thus, even though the efficacy of $[\mathbf{2}](PF_6)_2$ seemed to decrease in 3D compared to that in classical 2D tests, the higher $EC_{50}$ seems here to be the result of 3D spheroid testing, while the photochemical release of **1** by light irradiation of $[\mathbf{2}](PF_6)_2$ still leads, in 3D tumor spheroids, to a significantly increased cytotoxicity.

***In Vivo* (Photo)toxicity Studies.** The light activation observed in 2D cell monolayers and 3D tumor spheroids opened the door to testing the ability of photocaged drug $[\mathbf{2}](PF_6)_2$ to limit tumor cell proliferation *in vivo* using a xenograft model in nude mice, as previously described for PDT.[48] Considering the strong deactivation of $[\mathbf{2}](PF_6)_2$ in A431 tumor spheroids, compared to cell monolayers, the A549 cell line was preferred for testing in mice, as xenografts of this cell line may be less compact than those for A431, and thus offer better drug penetration *in vivo*. The tumors were produced by subcutaneous injection of A549 lung cancer cells. Each mouse carried two tumors as injections were made on each side of the mouse. In the group of irradiated mice, only one of the two tumors was irradiated with a green laser (520 nm, 40 mW, 38 J·cm$^{-2}$, 2 × 10 min irradiation) 24 h after compound injection. After treatment, tumor growth was followed daily. Before these experiments, very little information was available about which doses of PACT compounds may be used safely in mice. It was also unclear whether the compound should be injected intravenously, intraperitoneally, or directly into the tumor. In their original publication,[5] Kornienko et al. injected **1** intravenously at a dose of 3 mg·kg$^{-1}$ and 5 times per week intravenously, which would correspond, considering the


DOI: 10.1021/jacs.9b07225
J. Am. Chem. Soc. 2019, 141, 18444−18454

difference in molar weight between **1** and $[\mathbf{2}](PF_6)_2$, to a dose of caged inhibitor $[\mathbf{2}](PF_6)_2$ of 5 times at 9 mg·kg$^{-1}$ per week, which seemed very high. In a first experiment, $[\mathbf{2}](PF_6)_2$ was hence used at a low dose of 2 mg·kg$^{-1}$ injected intravenously. This treatment led to significant toxicity issues, with a quick death of the treated mice. In a second experiment, the doses of **1** and $[\mathbf{2}](PF_6)_2$ were hence reduced to 1 mg·kg$^{-1}$, and injections were made intraperitoneally.

With this new modality, we did not notice any significant toxicity of **1** or $[\mathbf{2}](PF_6)_2$: no mice appeared to lose weight or change behavior regardless of the treatment received (data not shown). The daily evolutions of the tumor size are shown in Figure 9. In the control group (mice treated with the vehicle), no significant difference was detected in tumor volume between the irradiated and nonirradiated tumors, indicating that green light irradiation alone had no effect on tumor growth ($p > 0.05$). In the group of mice treated with **1**, there was no significant difference on tumor volumes compared to that of control group ($p > 0.05$), while a clear antitumor activity had been observed at significantly higher doses (3 mg·kg$^{-1}$ per intravenous injection, 5 injections per week).[5] Therefore, at such low doses and using intraperitoneal injection, **1** did not alter tumor growth in either nonirradiated tumors or irradiated tumors. In the group of mice treated with $[\mathbf{2}](PF_6)_2$, nonirradiated tumors showed no significant decrease in tumor growth, while tumors photoactivated with green light showed significant slowing in tumor growth after 15 days, compared to untreated group (*, $p < 0.05$). At the end of the treatment, tumor volumes of mice treated with $[\mathbf{2}](PF_6)_2$ with subsequent green light irradiation were reduced by about 30%. Though significant, the effects observed after light irradiation are modest compared to results found in the literature with traditional ruthenium chemotherapy agents, i.e., compounds that are not activated by light.[49−51] However, it should be noted that since the effect obtained *in vitro* was significant, we chose to use *in vivo* doses that were also lower (1 mg/kg) than those in most other studies with anticancer ruthenium complexes (10−20 mg/kg in general),[49−51] regardless of the associated drugs. In addition, the dose-to-light interval of 24 h is rather long, and in such an interval, some of the compound might be eliminated before light activation occurs. Still, this *in vivo* study represents the proof-of-concept that ruthenium PACT compounds such as $[\mathbf{2}](PF_6)_2$ can be nontoxic in nude mice when injected intraperitoneally and lead to significant reduction of tumor growth upon irradiation with light. Obviously, these initial promising results will need to be completed by maximum tolerated dose and biodistribution studies, while the treatment protocol (injection mode, compound dose, dose-to-light delay, and light dose) should be optimized to increase antitumor efficacy.

## CONCLUSION

Our work demonstrates that microtubule-targeted thioether **1** can be caged by $[Ru(tpy)(bpy)]^{2+}$. *In vitro* green light photosubstitution of ruthenium-caged rigidin **1** in $[\mathbf{2}](PF_6)_2$ induces an up to a 29-fold increase in cytotoxicity under normoxia, with potencies that are similar to that of uncaged ligand **1**. The effect of light activation is still maintained in hypoxic lung or skin cancer cells and lung fibroblasts, where it is not linked to cell growth rates. We also demonstrated that $[\mathbf{2}](PF_6)_2$ can slow the growth of 3D tumor spheroids *in vitro* and A549 tumors *in vivo*, only after green light irradiation. As many microtubule-targeting agents are used in the clinic to treat cancer,[1,52,53] the strategy presented herein of ruthenium caging and green light photorelease provides a basis for a new cancer-targeted photoactivated chemotherapy for hypoxic tumors. This strategy is clearly distinct from the approach of organic chemists in photopharmacology, where azobenzene-functionalized protein inhibitors are switched "on" and "off" via cis−trans photoisomerization.[54−57] Coordination of an inhibitor to a light-sensitive metal complex, as proposed in this work, offers a promising alternative compared to the azobenzene isomerization approach developed by Feringa or Trauner among others. First, in photopharmacology the light activation wavelength is crucial. Low-energy green or red light can penetrate into tissues much deeper and is less harmful than high-energy UV or blue light. Although recently some azobenzenes have been developed that can be activated by visible or even red light,[58−60] ruthenium polypyridyl chemistry provides a well-understood, tunable, and predictive foundation for developing agents that can be activated by green or red light.[13,61−64] Second, as azobenzenes have a small or no dipole moment, especially in their trans form, they are highly lipophilic and often poorly water-soluble (typical log *P* values are ∼4).[65−67] Ruthenium complexes on the other hand are positively charged molecules, which provides enhanced water solubility of the caged compound $[\mathbf{2}](PF_6)_2$. Finally, light activation of metal-based PACT compounds usually entails an irreversible process, whereas cis−trans photoisomerization of azobenzenes is reversible. In the development of anticancer drugs both organic and inorganic chemists cope with similar problems, i.e., drug resistance, dose-limiting side effects, and poor water solubility. Here, activation in hypoxic conditions is clearly occurring, but under such conditions photoindices remain low *in vitro*. The combination of organic chemistry, which offers stable compounds and well-defined targets, with nontoxic inorganic photocaging compounds such as $[\mathbf{3}](PF_6)_2$, which lowers dark toxicity, increases water solubility, and allows for irreversible uncaging using visible light, demonstrates the complementarity between both disciplines. By crossing research borders, novel solutions will be found that can contribute to ground-breaking developments in the photopharmacology of hypoxic tumors.

## ASSOCIATED CONTENT

### Supporting Information

The Supporting Information is available free of charge on the ACS Publications website at DOI: 10.1021/jacs.9b07225.

Synthetic procedures, photochemical data (mass spectrometry, $^1$H NMR, UV−vis), tubulin polymerization assay, description of the cytotoxicity assay and cell culture in 2D, 2D cell growth curve experiments, cytotoxicity assay in 3D tumor spheroids, 2D and 3D cell irradiation protocols, and protocols for mice experiments (PDF)

## AUTHOR INFORMATION


### Corresponding Authors

*E-mail: bonnet@chem.leidenuniv.nl (S.B.).
*E-mail: a_k76@txstate.edu (A.K.).

### ORCID

Vincent Sol: 0000-0003-0175-0156
Sylvestre Bonnet: 0000-0002-5810-3657




DOI: 10.1021/jacs.9b07225
J. Am. Chem. Soc. 2019, 141, 18444−18454

### Notes

The authors declare no competing financial interest.

## ■ ACKNOWLEDGMENTS

The European Council is kindly acknowledged for financial support via a Proof-of-Concept grant (HypoRuLight) and a Starting Grant to S.B. NWO is kindly acknowledged for financial support via a VIDI grant to S.B. The financial support of the Haute-Vienne departmental committee of the "Ligue contre le Cancer" is kindly ackowledged. A.K. acknowledges the grant from the National Cancer Institute (CA186046-01A1). T.H. is grateful to the National Science Foundation (grant CHE-1552359).

## ■ REFERENCES

(1) Jordan, M. A.; Wilson, L. Microtubules as a target for anticancer drugs. *Nat. Rev. Cancer* **2004**, *4*, 253−265.
(2) Rowinsky, E. K.; Donehower, R. C. Paclitaxel (Taxol). *N. Engl. J. Med.* **1995**, *332*, 1004−1014.
(3) Salmela, A.-L.; Kallio, M. J. Mitosis as an anti-cancer drug target. *Chromosoma* **2013**, *122*, 431−449.
(4) Markman, M. Managing taxane toxicities. *Supportive Care in Cancer* **2003**, *11*, 144−147.
(5) Medellin, D. C.; Zhou, Q.; Scott, R.; Hill, R. M.; Frail, S. K.; Dasari, R.; Ontiveros, S. J.; Pelly, S. C.; van Otterlo, W. A. L.; Betancourt, T.; Shuster, C. B.; Hamel, E.; Bai, R.; LaBarbera, D. V.; Rogelj, S.; Frolova, L. V.; Kornienko, A. Novel Microtubule-Targeting 7-Deazahypoxanthines Derived from Marine Alkaloid Rigidins with Potent in Vitro and in Vivo Anticancer Activities. *J. Med. Chem.* **2016**, *59*, 480−485.
(6) Frolova, L. V.; Magedov, I. V.; Romero, A. E.; Karki, M.; Otero, I.; Hayden, K.; Evdokimov, N. M.; Banuls, L. M. Y.; Rastogi, S. K.; Smith, W. R.; Lu, S.-L.; Kiss, R.; Shuster, C. B.; Hamel, E.; Betancourt, T.; Rogelj, S.; Kornienko, A. Exploring Natural Product Chemistry and Biology with Multicomponent Reactions. 5. Discovery of a Novel Tubulin-Targeting Scaffold Derived from the Rigidin Family of Marine Alkaloids. *J. Med. Chem.* **2013**, *56*, 6886−6900.
(7) Sgambellone, M. A.; David, A.; Garner, R. N.; Dunbar, K. R.; Turro, C. Cellular Toxicity Induced by the Photorelease of a Caged Bioactive Molecule: Design of a Potential Dual-Action Ru(II) Complex. *J. Am. Chem. Soc.* **2013**, *135*, 11274−11282.
(8) Garner, R. N.; Gallucci, J. C.; Dunbar, K. R.; Turro, C. [Ru(bpy)2(5-cyanouracil)2]2+ as a potential light-activated dual-action therapeutic agent. *Inorg. Chem.* **2011**, *50*, 9213−5.
(9) Chan, H.; Ghrayche, J. B.; Wei, J.; Renfrew, A. K. Photolabile Ruthenium(II)−Purine Complexes: Phototoxicity, DNA Binding, and Light-Triggered Drug Release. *Eur. J. Inorg. Chem.* **2017**, *2017*, 1679−1686.
(10) Karaoun, N.; Renfrew, A. K. A luminescent ruthenium(ii) complex for light-triggered drug release and live cell imaging. *Chem. Commun.* **2015**, *51*, 14038−14041.
(11) Zayat, L.; Calero, C.; Albores, P.; Baraldo, L.; Etchenique, R. A new strategy for neurochemical photodelivery: Metal-ligand heterolytic cleavage. *J. Am. Chem. Soc.* **2003**, *125*, 882−883.
(12) Chen, Z.; Xiong, Y.; Etchenique, R.; Wu, S. Manipulating pH using near-infrared light assisted by upconverting nanoparticles. *Chem. Commun.* **2016**, *52*, 13959−13962.
(13) Mari, C.; Pierroz, V.; Ferrari, S.; Gasser, G. Combination of Ru(ii) complexes and light: new frontiers in cancer therapy. *Chem. Sci.* **2015**, *6*, 2660−2686.
(14) Huisman, M.; White, J. K.; Lewalski, V. G.; Podgorski, I.; Turro, C.; Kodanko, J. J. Caging the uncageable: using metal complex release for photochemical control over irreversible inhibition. *Chem. Commun.* **2016**, *52*, 12590−12593.
(15) Arora, K.; White, J. K.; Sharma, R.; Mazumder, S.; Martin, P. D.; Schlegel, H. B.; Turro, C.; Kodanko, J. J. Effects of Methyl Substitution in Ruthenium Tris(2-pyridylmethyl)amine Photocaging Groups for Nitriles. *Inorg. Chem.* **2016**, *55*, 6968−6979.
(16) Respondek, T.; Garner, R. N.; Herroon, M. K.; Podgorski, I.; Turro, C.; Kodanko, J. J. Light Activation of a Cysteine Protease Inhibitor: Caging of a Peptidomimetic Nitrile with Ru II(bpy) 2. *J. Am. Chem. Soc.* **2011**, *133*, 17164−17167.
(17) Dolmans, D. E. J. G. J.; Fukumura, D.; Jain, R. K. Photodynamic therapy for cancer. *Nat. Rev. Cancer* **2003**, *3*, 380−387.
(18) Triesscheijn, M.; Baas, P.; Schellens, J. H. M.; Stewart, F. A. Photodynamic Therapy in Oncology. *Oncologist* **2006**, *11*, 1034−1044.
(19) Karakullukcu, B.; Nyst, H. J.; van Veen, R. L.; Hoebers, F. J. P.; Hamming-Vrieze, O.; Witjes, M. J. H.; de Visscher, S. A. H. J.; Burlage, F. R.; Levendag, P. C.; Sterenborg, H. J. C. M.; Tan, I. B. mTHPC mediated interstitial photodynamic therapy of recurrent nonmetastatic base of tongue cancers: Development of a new method. *Head Neck* **2012**, *34*, 1597−1606.
(20) Allison, R.; Moghissi, K.; Downie, G.; Dixon, K. Photodynamic therapy (PDT) for lung cancer. *Photodiagn. Photodyn. Ther.* **2011**, *8*, 231−239.
(21) Gilkes, D. M.; Semenza, G. L.; Wirtz, D. Hypoxia and the extracellular matrix: drivers of tumour metastasis. *Nat. Rev. Cancer* **2014**, *14*, 430−439.
(22) Sun, W.; Wen, Y.; Thiramanas, R.; Chen, M.; Han, J.; Gong, N.; Wagner, M.; Jiang, S.; Meijer, M. S.; Bonnet, S.; Butt, H.-J.; Mailänder, V.; Liang, X.-J.; Wu, S. Red-Light-Controlled Release of Drug−Ru Complex Conjugates from Metallopolymer Micelles for Phototherapy in Hypoxic Tumor Environments. *Adv. Funct. Mater.* **2018**, *28*, 1804227.
(23) Lameijer, L. N.; Ernst, D.; Hopkins, S. L.; Meijer, M. S.; Askes, S. H. C.; Le Dévédec, S. E.; Bonnet, S. A red light-activated ruthenium-caged NAMPT inhibitor remains phototoxic in hypoxic cancer cells. *Angew. Chem., Int. Ed.* **2017**, *56*, 11549−11553.
(24) Rockwell, S.; Dobrucki, I. T.; Kim, E. Y.; Marrison, S. T.; Vu, V. T. Hypoxia and radiation therapy: past history, ongoing research, and future promise. *Curr. Mol. Med.* **2009**, *9*, 442−458.
(25) Cosse, J.-P.; Michiels, C. Tumour Hypoxia Affects the Responsiveness of Cancer Cells to Chemotherapy and Promotes Cancer Progression. *Anti-Cancer Agents Med. Chem.* **2008**, *8*, 790−797.
(26) Sullivan, R.; Pare, G. C.; Frederiksen, L. J.; Semenza, G. L.; Graham, C. H. Hypoxia-induced resistance to anticancer drugs is associated with decreased senescence and requires hypoxia-inducible factor-1 activity. *Mol. Cancer Ther.* **2008**, *7*, 1961−1973.
(27) Sitkovsky, M. V.; Kjaergaard, J.; Lukashev, D.; Ohta, A. Hypoxia-adenosinergic immunosuppression: tumor protection by T regulatory cells and cancerous tissue hypoxia. *Clin. Cancer Res.* **2008**, *14*, 5947−5952.
(28) Goldbach, R. E.; Rodriguez-Garcia, I.; van Lenthe, J. H.; Siegler, M. A.; Bonnet, S. N-acetylmethionine and biotin as photocleavable protective groups for ruthenium polypyridyl complexes. *Chem. - Eur. J.* **2011**, *17*, 9924−9.
(29) Lauffer, R. B. Paramagnetic metal complexes as water proton relaxation agents for NMR imaging: theory and design. *Chem. Rev.* **1987**, *87*, 901−927.
(30) Clore, G. M.; Iwahara, J. Theory, Practice, and Applications of Paramagnetic Relaxation Enhancement for the Characterization of Transient Low-Population States of Biological Macromolecules and Their Complexes. *Chem. Rev.* **2009**, *109*, 4108−4139.
(31) Bakhmutov, V. I. Strategies for Solid-State NMR Studies of Materials: From Diamagnetic to Paramagnetic Porous Solids. *Chem. Rev.* **2011**, *111*, 530−562.
(32) Bloembergen, N.; Purcell, E. M.; Pound, R. V. Relaxation Effects in Nuclear Magnetic Resonance Absorption. *Phys. Rev.* **1948**, *73*, 679−712.
(33) van Rixel, V. H. S.; Busemann, A.; Göttle, A. J.; Bonnet, S. Preparation, stability, and photoreactivity of thiolato ruthenium polypyridyl complexes: Can cysteine derivatives protect ruthenium-based anticancer complexes? *J. Inorg. Biochem.* **2015**, *150*, 174−181.


DOI: 10.1021/jacs.9b07225
*J. Am. Chem. Soc.* 2019, 141, 18444−18454

(34) Hopkins, S. L.; Siewert, B.; Askes, S. H. C.; Veldhuizen, P.; Zwier, R.; Heger, M.; Bonnet, S. An in vitro cell irradiation protocol for testing photopharmaceuticals and the effect of blue, green, and red light on human cancer cell lines. *Photochem. Photobiol. Sci.* **2016**, *15*, 644−653.
(35) Siewert, B.; van Rixel, V. H. S.; van Rooden, E. J.; Hopkins, S. L.; Moester, M. J. B.; Ariese, F.; Siegler, M. A.; Bonnet, S. Chemical Swarming: Depending on Concentration, an Amphiphilic Ruthenium Polypyridyl Complex Induces Cell Death via Two Different Mechanisms. *Chem. - Eur. J.* **2016**, *22*, 10960−10968.
(36) McMillan, T. J.; Leatherman, E.; Ridley, A.; Shorrocks, J.; Tobi, S. E.; Whiteside, J. R. Cellular effects of long wavelength UV light (UVA) in mammalian cells. *J. Pharm. Pharmacol.* **2008**, *60*, 969−976.
(37) Wäldchen, S.; Lehmann, J.; Klein, T.; van de Linde, S.; Sauer, M. Light-induced cell damage in live-cell super-resolution microscopy. *Sci. Rep.* **2015**, *5*, 15348.
(38) Wilson, W. R.; Hay, M. P. Targeting hypoxia in cancer therapy. *Nat. Rev. Cancer* **2011**, *11*, 393.
(39) Muz, B.; de la Puente, P.; Azab, F.; Azab, A. K. The role of hypoxia in cancer progression, angiogenesis, metastasis, and resistance to therapy. *Hypoxia* **2015**, 83−10.
(40) Vichai, V.; Kirtikara, K. Sulforhodamine B colorimetric assay for cytotoxicity screening. *Nat. Protoc.* **2006**, *1*, 1112−1116.
(41) Hubbi, M. E.; Semenza, G. L. Regulation of cell proliferation by hypoxia-inducible factors. *American Journal of Physiology-Cell Physiology* **2015**, *309*, C775−C782.
(42) Wulftange, W. J.; Rose, M. A.; Garmendia Cedillos, M.; da Silva, D.; Poprawski, J. E.; Srinivasachar, D.; Sullivan, T.; Lim, L.; Bliskovsky, V. V.; Hall, M. D.; Pohida, T. J.; Robey, R. W.; Morgan, N. Y.; Gottesman, M. M. Spatial control of oxygen delivery to three-dimensional cultures alters cancer cell growth and gene expression. *J. Cell. Physiol.* **2019**, *234*, 20608−20622.
(43) Yu, L.; Hales, C. A. Long-term exposure to hypoxia inhibits tumor progression of lung cancer in rats and mice. *BMC Cancer* **2011**, *11*, 331.
(44) White, E. S. Lung Extracellular Matrix and Fibroblast Function. *Ann. Am. Thorac. Soc.* **2015**, *12*, S30−S33.
(45) He, Z. P.; Xie, M. Curcumin inhibits hypoxia-induced proliferation of MRC-5 and collagen I synthesis. *Sichuan Da Xue Xue Bao, Yixueban* **2010**, *41*, S30−S33 (in Chinese) .
(46) Senavirathna, L. K.; Huang, C.; Yang, X.; Munteanu, M. C.; Sathiaseelan, R.; Xu, D.; Henke, C. A.; Liu, L. Hypoxia induces pulmonary fibroblast proliferation through NFAT signaling. *Sci. Rep.* **2018**, *8*, 2709.
(47) Petrova, V.; Annicchiarico-Petruzzelli, M.; Melino, G.; Amelio, I. The hypoxic tumour microenvironment. *Oncogenesis* **2018**, *7*, 1−13.
(48) Fidanzi-Dugas, C.; Liagre, B.; Chemin, G.; Perraud, A.; Carrion, C.; Couquet, C.-Y.; Granet, R.; Sol, V.; Léger, D. Y. Analysis of the in vitro and in vivo effects of Photodynamic Therapy on Prostate Cancer by using new photosensitizers, protoporphyrin IX-polyamine derivatives. *Biochim. Biophys. Acta, Gen. Subj.* **2017**, *1861*, 1676−1690.
(49) Chen, L.; Li, G.; Peng, F.; Jie, X.; Dongye, G.; Cai, K.; Feng, R.; Li, B.; Zeng, Q.; Lun, K.; Chen, J.; Xu, B. The induction of autophagy against mitochondria-mediated apoptosis in lung cancer cells by a ruthenium (II) imidazole complex. *Oncotarget* **2016**, *7*, 80716−80734.
(50) Alves de Souza, C. E.; Alves de Souza, H. d. M.; Stipp, M. C.; Corso, C. R.; Galindo, C. M.; Cardoso, C. R.; Dittrich, R. L.; de Souza Ramos, E. A.; Klassen, G.; Carlos, R. M.; Correia Cadena, S. M. S.; Acco, A. Ruthenium complex exerts antineoplastic effects that are mediated by oxidative stress without inducing toxicity in Walker-256 tumor-bearing rats. *Free Radical Biol. Med.* **2017**, *110*, 228−239.
(51) Zhang, G.; Wu, C.; Ye, H.; Yan, H.; Wang, X. Nanoscaled carborane ruthenium(II)-arene complex inducing lung cancer cells apoptosis. *J. Nanobiotechnol.* **2011**, *9*, 6.
(52) Prasad, S.; Gupta, S. C.; Aggarwal, B. B. Serendipity in Cancer Drug Discovery: Rational or Coincidence? *Trends Pharmacol. Sci.* **2016**, *37*, 435−450.
(53) Chan, K. S.; Koh, C. G.; Li, H. Y. Mitosis-targeted anti-cancer therapies: where they stand. *Cell Death Dis.* **2012**, *3*, e411.
(54) Broichhagen, J.; Frank, J. A.; Trauner, D. A Roadmap to Success in Photopharmacology. *Acc. Chem. Res.* **2015**, *48*, 1947−1960.
(55) Velema, W. A.; Szymanski, W.; Feringa, B. L. Photopharmacology: Beyond Proof of Principle. *J. Am. Chem. Soc.* **2014**, *136*, 2178−2191.
(56) Dong, M.; Babalhavaeji, A.; Samanta, S.; Beharry, A. A.; Woolley, G. A. Red-Shifting Azobenzene Photoswitches for in Vivo Use. *Acc. Chem. Res.* **2015**, *48*, 2662−2670.
(57) Schönberger, M.; Trauner, D. A Photochromic Agonist for μ-Opioid Receptors. *Angew. Chem., Int. Ed.* **2014**, *53*, 3264−3267.
(58) Samanta, S.; Qin, C.; Lough, A. J.; Woolley, G. A. Bidirectional Photocontrol of Peptide Conformation with a Bridged Azobenzene Derivative. *Angew. Chem., Int. Ed.* **2012**, *51*, 6452−6455.
(59) Samanta, S.; McCormick, T. M.; Schmidt, S. K.; Seferos, D. S.; Woolley, G. A. Robust visible light photoswitching with ortho-thiol substituted azobenzenes. *Chem. Commun.* **2013**, *49*, 10314−10316.
(60) Lerch, M. M.; Hansen, M. J.; Velema, W. A.; Szymanski, W.; Feringa, B. L. Orthogonal photoswitching in a multifunctional molecular system. *Nat. Commun.* **2016**, *7*, 12054.
(61) Bonnet, S. Shifting the Light Activation of Metallodrugs to the Red and Near-Infrared Region in Anticancer Phototherapy. *Comments Inorg. Chem.* **2015**, *35*, 179−213.
(62) Crespy, D.; Landfester, K.; Schubert, U. S.; Schiller, A. Potential photoactivated metallopharmaceuticals: from active molecules to supported drugs. *Chem. Commun.* **2010**, *46*, 6651−6662.
(63) Knoll, J. D.; Turro, C. Control and utilization of ruthenium and rhodium metal complex excited states for photoactivated cancer therapy. *Coord. Chem. Rev.* **2015**, *282*−*283*, 110−126.
(64) Farrer, N. J.; Salassa, L.; Sadler, P. J. Photoactivated chemotherapy (PACT): the potential of excited-state d-block metals in medicine. *Dalton Trans.* **2009**, 10690−10701.
(65) Brown, C.; Rastogi, S. K.; Barrett, S. L.; Anderson, H. E.; Twichell, E.; Gralinski, S.; McDonald, A.; Brittain, W. J. Differential azobenzene solubility increases equilibrium cis/trans ratio in water. *J. Photochem. Photobiol., A* **2017**, *336*, 140−145.
(66) Du, C. M.; Valko, K.; Bevan, C.; Reynolds, D.; Abraham, M. H. Rapid method for estimating octanol-water partition coefficient (log Poct) from isocratic RP-HPLC and a hydrogen bond acidity term (A). *J. Liq. Chromatogr. Relat. Technol.* **2001**, *24*, 635−649.
(67) Huuskonen, J. Prediction of Soil Sorption Coefficient of a Diverse Set of Organic Chemicals From Molecular Structure. *J. Chem. Inf. Comput. Sci.* **2003**, *43*, 1457−1462.


DOI: 10.1021/jacs.9b07225
*J. Am. Chem. Soc.* 2019, 141, 18444−18454